In situ Test Method for the Electrostatic Characterization of Lunar Dust

Buhler, C.R.[1], Calle, C.I.[2], Clements, S.J.[3], Mantovani, J.[2], and Ritz, M.L.[1]

[1]ASRC Aerospace, Kennedy Space Center, FL 32899, USA
[2]NASA, KT-E, Kennedy Space Center, FL 32899,USA
[3]Department of Physics and Astronomy, Appalachian State University,
Boone, NC 28608, USA

Abstract – This paper serves to illustrate the testing methods necessary to classify the electrostatic properties of lunar dust using in situ instrumentation and the required techniques therein. A review of electrostatic classification of lunar simulant materials is provided as is its relevance to the success of future human lunar missions.

Key words: Lunar dust, electrostatics, granular materials, volume resistivity, charge decay, charge-to-mass, chargeability and dielectric constant.

Table of Contents

1.0 Introduction

In response to President Bush's Vision for Exploration Initiative, NASA created the Constellation Program which aims to send humans back to the Moon and onto Mars. However, the two most important measurements yet to be made on the lunar surface regarding the safety and success of these missions is the toxicity of the lunar dust and its electrostatic properties.

The toxicity of the soil is of vital interest due to the obvious health hazard to the astronauts. The amount of toxicity is governed by several factors including the particle size, shape, and chemical reactivity. If the particles are the correct size, they will lodge themselves into the lungs, clogging pores and perhaps penetrate directly into the blood stream. Furthermore, if the particles are jagged and of irregular shape, they may be abrasive and damaging to tissue in the lungs, eyes, throat, etc... Finally, if the particles are chemically reactive they may serve to react with skin or internal organs which could lead to serious problems.

The relevance of the electrostatic properties are less obvious but equally important. The electrostatic properties of dust essentially govern its behavior including everything from lung deposition to surface contamination. The lunar dust attached to every surface that came in contact with it during the Apollo missions. The astronauts struggled and fought the dust constantly throughout the traverses on the surface as well as in the lunar module on the return trip home. It was Astronaut Harry Schmidt that said, "Dust is going to be *the* environmental problem for future missions, both inside and outside the habitats." The dust is such a problem that NASA has selected the dust mitigation strategy as one of its top two problems that need to be solved before returning to the Moon. It is this property that this paper addresses.

Dust adherence caused visual obscuration, false instrument readings, loss of traction, clogging of mechanisms, abrasion, thermal control problems, seal failures, and coating of nearly all surfaces during the Apollo missions. Dust adhered to the astronaut's boots, suits, visors, etc., entered into the lunar module and eventually the command module then became aerosolized and created inhalation and irritation problems.

There are many causes for dust adherence but we will show that the main proponent of dust adherence on the Moon is electrostatics. There are four known forces responsible for dust adherence: Van der Waal forces, capillary forces, mechanical forces and electrostatic forces. Van der Waal forces are strongest of all known forces, however, the range of this force falls off as $1/r^6$ with distance meaning that it is only important for extremely small particles (< 1 μm) that are extremely close to very smooth surfaces (less than 10^{-10} m). When a dust particle sits on a surface it is likely that the force only acts on the part of the particle that is within the Van der Waal range while a significant portion of the particle will not experience this force if it has any noticeable size (>1 μm) and is deposited onto a rough surface. Capillary forces are adherence forces resulting from surface tension of moisture between the particle and the surface. In the case for the Moon (or Mars) the amount of moisture on the surface of the particles is most likely zero and this force does not apply. Mechanical forces arise from plastic deformation or jagged particles fitting in the groves on the surface of materials. This is an unlikely force of adhesion since the lunar dust is very hard and it is unlikely that particles are capable of plastic deformation.

The remaining significant force on the dust particles responsible for adhesion is the electrostatic force. Electrostatic forces act on any particle that has a charge through the Coulomb force

$$F = QE$$

and acts on any uncharged particles through the dielectrophoretic (DEP) force

$$\left\langle \vec{F} \right\rangle = \frac{1}{2}\mathrm{Re}\left[\left(\vec{p}\cdot\vec{\nabla}\right)\cdot\vec{E}^{*}\right]$$

in the presence of a spatially nonuniform and/or temporarily time dependent electric field where $\vec{E}^{*}$ is the complex conjugate of the electric field and $\vec{p}$ is the induced electric dipole moment. For spherical particles the dipole moment becomes

$$\vec{p} = 4\pi\varepsilon_m a^3 f_{CM}\vec{E}$$

where ε_m is the permittivity of the medium, a is the particle radius, and f_{CM} is the Clausius-Mossotti factor given by:

$$f_{CM} = \frac{\varepsilon_p^{*} - \varepsilon_m^{*}}{\varepsilon_p^{*} + 2\varepsilon_m^{*}}.$$

Here ε_p^{*} and ε_m^{*} are the complex permittivities of the particle and medium, respectively. The electrostatic force acts on particles on all three regimes: near, far and mid range and is applicable to the Moon, Mars as well as Earth. The electrostatic properties of the dust are exasperated because of the dry conditions of the lunar surface. It was this property of the dust that leads to its adherence qualities as confirmed by the Apollo 12 Mission Briefing Report on page 6-5 that stated "the cohesive properties of the lunar dust in vacuum, augmented by electrostatic properties, tend to make it adhere to anything it contacts".

There are several methods available to charge the dust on the Moon such as plasma charging by thermal electrons and protons from the solar wind, photoemission from solar ultraviolet and soft X-rays, photoelectron charging of particles suspended within the photoelectron sheath, the impact of highly energetic electrons captured in the Earth's magnetotail and galactic cosmic rays. However the greatest charge generation mechanism of major concern on the Moon during future lunar exploration is triboelectrification or the generation of charge due to contact and separation of materials. The action of mechanical movements is enough to significantly charge dust regardless of the materials it comes in contact with.

Therefore the key questions in solving the dust problem on the Moon is 1) how much charge can accumulate on the dust, 2) how long will the charge remain and 3) can the dust be removed using both conventional and unconventional methods?

1.1 Volume resistivity

These questions can only be answered by fully classifying the electrostatic properties of the dust which includes: volume resistivity, charge decay, charge-to-mass ratio or chargeability and dielectric properties. For example knowledge of the volume resistivity of the material gives an indication of the likelihood for the particles to acquire charge and their ability to dissipate said charge. Materials with high volume resistivities such as *insulators* typically have resistivities higher than 10^9 Ωm and usually acquire larger amounts of charge during triboelectrification.

They also sustain that charge longer than *statically dissipative* materials with resistivities between 10^6 and 10^9 Ωm and *conductive* materials with resistivities below 10^6 Ωm.

Measurements typically involve placing the sample between two electrodes, applying a known voltage V and monitoring the resulting current I. The volume resistivity is

$$R_V = \frac{V}{I}\frac{A}{d}$$

where A is the electrode area and d is the sample thickness. Volume resistivity values are only successful if there is a steady current for the applied voltage which ranges from 100 volts up to 10 kV depending upon the expected resistivity values.

There have been several studies performed on the DC electrical resistivity of the lunar samples which range from 10^{14} Ωm for soils to 10^9 Ωm for rocks in the absence of light and moisture [1]. The addition of both light and moisture can give up to 10^6 decrease in magnitude of the resistivity [2]. The temperature dependent form for the DC electrical conductivity σ (the inverse of resistivity) was found by Olhoeft [3] to be

$$\sigma = 6\times10^{-18}e^{0.0237T}\ \text{mho/m}$$

which is characteristic of the amorphous agglutinates that make up the lunar soil particles and matches well with extremely dry terrestrial silicates. The volume resistivity measurements of lunar fines performed by several investigators have shown that the materials are highly insulating illustrating the conduction is perhaps due to ionic rather than electronic mechanisms in the absences of moisture. Metallic conduction is thought to be unlikely due to the small amounts of free metals and metallic oxides present. Furthermore, the semiconducting oxide minerals such as ilmenite and iron oxides that contribute up to 20% of the lunar samples by volume are not responsible for conductivity due to their fine dispersion in the predominantly silicate matrix [3]. It is the highly insulating silicates that are the main phases responsible for conductivity observed in the lunar samples. For a complete review of electrical conductivity tests performed on all lunar samples see [4].

1.2 Charge Decay

Charge decay measurements are performed to measure the time it takes for samples to dissipate applied charge. For "simple" or Ohmic materials, those that are isotropic (polarization points in the direction of the electric field), homogeneous (no spatial gradients in the permittivity and conductivity) and linear (permittivity is not a function of electric field), the charge density of the material as a function of time can be found using both the continuity equation and Gauss's Law. For a net charge density ρ Gauss's Law is given by

$$\rho = \varepsilon\vec{\nabla}\cdot\vec{E}$$

where ε is the permittivity and $\vec{E}$ is the electric field. The continuity equation in the absences of sources or sinks is

$$\frac{\partial\rho}{\partial t} + \vec{\nabla}\cdot\vec{J} = 0.$$

Substituting Ohm's Law given as $\vec{J} = \sigma\vec{E}$ with σ as the conductivity into the above equation gives

$$\frac{\partial \rho}{\partial t} + \sigma \vec{\nabla} \cdot \vec{E} + \vec{E} \cdot \vec{\nabla} \sigma = 0 .$$

Making use of homogeneity for simple materials means $\nabla \sigma = 0$ and $\nabla \varepsilon = 0$ which reduces the continuity equation to

$$\frac{\partial \rho}{\partial t} + \sigma \frac{\rho}{\varepsilon} = 0 .$$

Integrating this equation from time $t = 0$ when the charge density is ρ_o at time t gives

$$\rho(t) = \rho_o \exp\left({}^{-t}\!/_{\tau_c} \right)$$

where $\tau_c = \varepsilon / \sigma$ is the intrinsic relaxation time of the conductor also called the charge decay time constant. The charge relaxation equation has the simple exponential decay form for Ohmic materials.

In simple circuits Ohms law is written as $V = IR$ (V is voltage, I is current, R is resistance) and charge decay can be computed by substituting $Q = VC$ (Q is the charge, C is the capacitance) and $I = dQ/dt$. The result of the charge remaining at a later time is given by $Q = Q_o e^{-t/\tau}$ where Q_o is the initial charge and $\tau = RC$, also known as the charge decay constant, is the time it takes for Q_o to reach 37% or $1/e$ of its value. Since the charge decay constant is a function of the resistance, measurements of volume resistivity is thought to correspond directly to the time it takes the material to dissipate its charge. However, since granular materials (and insulators in general) rarely exhibit pure Ohmic electrical characteristics, it is not always true that charge decay properties follow this simple decay behavior.

Experimentally, charge decay constants are measured by placing a charge on the material and monitoring either the charge dissipation $Q = Q_o e^{-t/\tau}$ or the surface potential decay $V = V_o e^{-t/\tau}$ with time. There are also several methods to apply charge to a material including, corona charging, electron beam charging, triboelectric charging and induction charging although some of these methods may be unsuitable for granular materials. This is a vital measurement that can be made directly that tells how quickly charge dissipates from the material.

For most materials the form of the charge decay is not a simple Ohmic decay behavior as seen for purely capacitive and resistive systems. Here the data is best fit by a more generalized approach described by Seaver [5] who considers separating intrinsic charge of a material with extrinsic charge placed on the material as a perturbation. In this case the charge density and the conductivity can be replaced by

$$\rho = \rho_m + \rho_p$$

$$\sigma = \sigma_m + \sigma_p = \sigma_m + \rho_p b_p .$$

Since the materials are uncharged initially $\rho_m = 0$ and only perturbations of charge density need be considered. The conductivity perturbation is simply the charge density perturbation ρ_p times the charge mobility b_p of the extrinsic charge. Substituting these into the continuity equation becomes

$$\frac{\partial \rho_p}{\partial t} + \frac{\sigma_m}{\varepsilon}\rho_p + \frac{b_p}{\varepsilon}\rho_p^2 = 0 .$$

The material's time constant can be defined with the intrinsic conductivity (1/resistivity) as

$$\tau_m = \frac{\varepsilon}{\sigma_m} = R_v \varepsilon$$

and a new constant in the third term can be defined as

$$\beta = \frac{b_p}{\varepsilon} .$$

The new form of the partial differential equation becomes

$$\frac{\partial \rho_p}{\partial t} + \frac{\rho_p}{\tau_m} + \beta \rho_p^2 = 0$$

to which the solution is

$$\frac{\beta \tau_m \rho_p}{\beta \tau_m \rho_p + 1} = \frac{\beta \tau_m \rho_{p0}}{\beta \tau_m \rho_{p0}} \exp\left(-t/\tau_m\right).$$

Now define a second time constant based on the initial perturbation as

$$\tau_p = \left(\beta \rho_{p0}\right)^{-1} = \frac{\varepsilon}{b_p \rho_{p0}} .$$

Thus the generalized charge decay equation that can be applied for materials becomes

$$\rho_p(t) = \frac{\rho_{p0} \exp\left(-t/\tau_m\right)}{1 + \frac{\tau_m}{\tau_p}\left[1 - \exp\left(-t/\tau_m\right)\right]} = \frac{\rho_{p0}}{\left(1 + \frac{\tau_m}{\tau_p}\right)\exp\left(t/\tau_m\right) - \frac{\tau_m}{\tau_p}} .$$

For a good conductor the intrinsic conductivity must be larger than the conductivity of the perturbation. This can be accommodated by making the second term in the continuity equation larger than the third equation as $\rho_p/\tau_m >> \beta \tau_m \rho_p$ or $1 >> \beta \tau_m \rho_{p0}$ since that largest value of ρ_p is ρ_{p0}. With the aid of the second time constant the criteria for a good conductor is $\tau_p >> \tau_m$ and the charge density reduces to

$$\rho_p(t) \approx \rho_{p0} \exp(-t/\tau_m)$$

which is exactly the form of Ohmic charge decay as before.

The reverse conditions are true for the case of a good insulator in which the second term in the continuity equation must be smaller than the third term giving $\rho_p/\tau_m << \beta \tau_m \rho_p$ or $1 >> \beta \tau_m \rho_p$. However, this can only be satisfied at early times since as $t \to \infty$ so must ρ_p and thus $1 >> \beta \tau_m \rho_p$ always fails. Therefore, the requirements can only be met at early time and the highest value of ρ_p is ρ_{p0} so the criteria for a good insulator is again $1 >> \beta \tau_m \rho_p$. Using the aid of the second time constant the criteria for a good insulator becomes $\tau_p << \tau_m$ and the charge density has the form

$$\rho_p(t) \approx \frac{\rho_{p0}}{\left(1+\frac{t}{\tau_p}\right)}$$

which is only valid for $\tau_p << \tau_m$ and if $t << \tau_m$. This equation has the familiar form of the hyperbolic law of Bustin [6]. This result can also be derived by replacing Ohm's Law $\vec{J} = \sigma \vec{E}$ with the diffusion law $\vec{J} = \rho \vec{u}$ where $\rho = \vec{\nabla} \cdot \vec{D}$ is the charge density derived from Gauss' Law and $\vec{u}$ is the velocity [7]. This form of charge decay behavior for lunar and Martian simulant materials was seen previously in our work [8, 9]. Simulants were charged using a corona source charged to ±10 kV source and the resulting surface potential was monitored using a single device called a JCI 155v4 Charge Decay Test Unit [10]. Experiments verified that the simulants were highly insulating with charge decay time constants longer than several hours.

1.3 Chargeability Measurements

Measurements of the charge-to-mass ratio, also called chargeability, are also performed on granular materials to determine the expected amount of charge acquired during a certain process. The charge-to-mass density of *individual* lunar dust particles is of vital interest for planetary scientists trying to understand some of the fundamental science questions posed by the Apollo missions such as the mysterious Horizon Glow. This glow is thought to be a result of reflected sunlight from levitated dust particles from a few centimeters to a few meters off of the surface of the Moon. One of the leading theories is that the dust is charged positively by the solar UV and soft X-rays through photoemission resulting in a surface potential of ~+10 volts. The precipitated electrons form a negatively charged photoelectron sheath with a thickness given by a characteristic Debye length from the surface which attracts the positively charged dust particles lifting them from the surface. During the lunar nights, the photoelectron sheath disappears and an abundance of electrons from solar wind charges the surface negatively with potentials on the order of ~-100 volts. Instrumentation on the lunar surface such as the Apollo Suprathermal Ion Detector Experiment (SIDE) [11] recorded the values of the surface potential while the data taken from the Lunar Ejecta and Meteorites (LEAM) Experiment [12] confirmed incidents of charged dust particle transport above the surface.

An excellent theoretical study as well as experimental confirmation of this model by [13] is illustrated below to reinforce the importance of electrostatics in the lunar environment. The model shows that it is indeed possible for dust particles to charge, lift and transport across the lunar surface and provides constraints for size and charge of suspended particles.

When dust particles are subject to UV light, the charging potential of an isolated grain due to the photoelectric effect is given by

$$V_{PE} = (E_\gamma - W)/e$$

where e is the elementary charge, E_γ is the energy of the solar spectrum (typically dominated by the Lyman-alpha emission of $\lambda = 121.6$ nm and $E_\gamma = 10.2$ eV) and W is the work function of the

particle ~5.8 eV. Electrons are given off which creates a photoelectron sheath characterized by its Debye length

$$\lambda_D = \sqrt{\frac{\varepsilon_o E_{pe}}{4\pi n_o e}}$$

and has a photoelectron density of

$$n = n_o\left(1+\frac{z}{\sqrt{2}\lambda_D}\right)^{-2}$$

at a height z above the surface, where E_{pe} is the photoelectron energy distribution in eV (~6 eV) and n_o is the photoelectron density at the surface (~60 cm^{-3}) giving an effective Debye length $\lambda_D \approx 66\,\text{cm}$. There is an unstable equilibrium height to which particles can levitate to within the photoelectron sheath [14];[15] a height roughly equivalent to the Debye length.

If the positively charged dust particle rises off to within the photoelectron sheath the electrostatic charge on the particle can be neutralized or it can begin to acquire a negative charge. In the presence of a negatively charged photoelectron sheath, the negatively charged particles are now accelerated toward the surface or above the sheath. If the particle rises above the photoelectron sheath, then plasma charging and photoemission become competing processes. Plasma charging is comprised of two currents, the thermal electron current given by

$$I_e = -\pi a^2 n_o e\sqrt{\frac{8E_e}{\pi m_e}}\exp\left[\frac{e\Phi_d}{E_e}\right]$$

and the ion current is

$$I_i = \pi a^2 n_o e\exp\left(-\frac{1}{2}\right)\sqrt{\frac{E_e}{m_i}}\left[1-\frac{e\Phi_d}{E_i}\right]$$

where a is the particle radius, n_o is the ion and electron current density (~60 cm^{-3}), $E_e = kT_e$ is the electron temperature, k is the Boltzmann constant, $E_i = 1/2 m_i v_i^2$ is the ion kinetic energy, and m_i and m_e are the ion and electron masses. In the presence of the space plasma the potential Φ_d of the particle, is found by setting the total current equal to zero. Once the potential Φ_d is known, the resulting charge on the grain is

$$Q = C\Phi_d = 4\pi\varepsilon_o a\Phi_d\,.$$

There was good agreement between the charge calculated from the above plasma model and the experimental value of charge measured using the force balance equation [16], [17]

$$\frac{4}{3}\pi a^3\rho g = -QE = -4\pi\varepsilon_o a\Phi_d(z)\frac{\partial\Phi(z)}{\partial z}$$

when considering the plasma charging case only. Grains were charged negatively through an artificial plasma source and levitated above a negatively biased electric field. The gradient of the sheath potential is determined by the plasma measurements so the particle potential Φ_d can be computed for comparison to the known currents to the particle.

Furthermore, we can calculate the second stable equilibrium height if we know the functional form of E in above the photoelectron sheath given by [18]

$$E(z) = E_o\left[1+\frac{z}{\sqrt{2}\lambda_D}\right]^{-1}$$

which can be substituted in the force balance equation to give the upper equilibrium height

$$z_{eq} = \sqrt{2}\lambda_D\left[\frac{3\varepsilon_o E_o \Phi_{sw}}{\rho g a^2} - 1\right].$$

Here the particles are assumed to have a potential Φ_{sw} due solely to the solar wind, ρ is the particle density (~3 g/cm^3), g is the lunar gravity, and a is their radius. The equilibrium height increases rapidly for small particles. The maximum size particle that can be stably levitated as a function of height is

$$a_{\max} = 4.98\left(\frac{E_o \Phi_{sw}}{4890z + 4564}\right)^{1/2} \text{ μm.}$$

Thus the minimum condition required for levitation is that particles be smaller than

$$a_{\max} = 0.074\sqrt{E_o \Phi_{sw}}\,.$$

For a typical surface electric field of 10 V/m with the particle's potential due to the solar wind only (typically $\Phi_{sw} \approx 4.5$ volts), the largest particles that can be levitated have a radii of ~0.5 μm. This corresponds to a particle with a charge $Q = 2.53\times10^{-16}$ C and a very high charge-to-mass ratio of $Q/m = 1.61\times10^{4}$ μC/kg.

Not only will individual dust particles obtain high electrostatic charging in the natural lunar environment, interaction of astronauts and equipment with the soil will provide electrostatic charging not only to the dust grains but to large quantities of bulk material as well. Unlike the charge-to-mass density of individual dust grains, the charge-to-mass density of bulk lunar soils has not been measured to our knowledge. This is of vital interest to future astronauts and explorers whose work will be more intense and of longer duration on the lunar surface. The future of lunar exploration will involve more handling, pouring, sieving, delivering, conveying, digging and grinding large quantities of lunar regolith which will result in undoubtedly higher electrostatic charging of soils than natural methods by the several new types of triboelectric charge generation. Typical charge-to-mass ratios of bulk powder materials by different handling operations for terrestrial conditions are given in Table 1 below.

Table 1. Charge generation on bulk powders [19]

Operation	Mass charge density (charge-to-mass ratio) μC/kg
Sieving	10^{-3} to 10^{-5}
Pouring	10^{-1} to 10^{-3}
Scroll feed transfer	1 to 10^{-2}
Grinding	1 to 10^{-1}
Micronizing	10^{2} to 10^{-1}
Pneumatic conveying	10^{3} to 10^{-1}

Classification of the charge mass densities of bulk granular materials is measured directly using a Faraday Cup which isolates the electric field of the charged particle from its surroundings. This

is an accurate measurement of charge that does not require knowledge of the capacitance of the system, which is usually a major source of error when utilizing surface potential techniques.

1.4 Dielectric Measurements

The most studied of all electrostatic properties are the dielectric properties or the dielectric permittivity. This is a measure of the ability of the material to physically separate its inherent charge, it is also called polarization. Normally the dielectric permittivity can be separated into its real and imaginary parts $\kappa = \kappa' + i\kappa''$ and

$$\tan\delta = \frac{\kappa''}{\kappa'}$$

is the loss tangent. The real part of the dielectric permittivity sometimes called the dielectric constant κ' is the ratio of the permittivity of the material ε divided by the permittivity of free space ε_o. Olhoeft and Strangway [4] have compiled a list of all of the dielectric measurements performed on all of the lunar samples up to 1975. Their analysis concluded that the dielectric constant depended mostly on the density of the sample ρ with the relation

$$\kappa' = (1.93 \pm 0.17)^{\rho}$$

and the loss tangent depends on only the density and the percentage of total FeO + TiO_2 (ilmenite) content C by

$$\tan\delta = [(0.00053 \pm 0.00056) + (0.00025 \pm 0.00009)C]\rho .$$

With such low loss tangents, radio waves are expected to transmit easily through the lunar surface. The real part of the permittivity (dielectric constant) is found to be between 3 and 5. Unlike the conductivity, neither the dielectric constant nor the loss tangent was found to vary significantly with the temperature observed during the lunar day.

1.5 In Situ Characterization

The seals of all Sample Return Containers brought back from the Apollo lander Moon missions were compromised, meaning that all of the lunar dust samples were contaminated by air. Although contamination by air does not affect many of the soils properties, it most likely affected the electrostatic properties to a certain extent. Oxidation is of one important consequence of exposure to ambient air. The addition of oxygen atoms to surface changes the surface chemistry, lowers the surface free energy, and changes the work function of the material. The work function is the energy required to remove an electron from bulk of the material. In many cases it is the work function that influences the magnitude and sign of charges exchanged between materials which govern their electrostatic charging properties. The work function changes dramatically from material to material except for oxidized metals which consistently have work functions about 5.5 eV. Thus the true nature of electrostatic charging of dust on the lunar surface remains unknown.

Another contaminate in the lunar samples that affects electrostatic properties is the addition of moisture upon exposure to ambient air. Although thought to be a reversible process, the heating of lunar samples to temperatures high enough to remove water contamination may inherently cause other unwanted effects such as chemical or compositional changes. The possibility of

microscopic melting of crystalline structures into smoother grains could have a detrimental affect on electrostatic properties in which geometry also plays an important role. Furthermore, although heating lunar regolith samples removes a bulk of the moisture it will undoubtedly leave moisture behind in the form of surface contamination, unless properly stirred, from the outgassing process onto other particles. Even the smallest amount of moisture can have dramatic affects on the electrostatic properties of soils and dusts. Oxidation and water adsorption are only two examples of how samples brought back from the lunar surface may have been contaminated.

All of above leads to the importance of *in situ* classification of the electrostatic properties of lunar regolith. Experiments performed under laboratory conditions may have been subject to contamination which can significantly alter the electrostatic properties of the dust.

2.0 Experimental Section

Electrostatic classification of lunar dust *in situ* has not been done and the techniques are not well known. To this end, we have developed a single device, part of a lander or rover for future lunar missions that is able to measure all four electrostatic properties: volume resistivity, charge decay, chargeability and dielectric permittivity. Two prototypes, or test cells, were used during experiments. An early version of the test cell called "Old Test Cell" used for previous research was built to comply with ASTM Standard D 150 for measurements of permittivity [20]. A later version with removable plates called "New Test Cell" was built to comply with both the ASTM Standard D 150 as well as British Standard (BS) 5958 for the measurement of the volume resistivity of powders [19]. Figure 1 shows the general test cell requirements that consist of a guard (green), a guarded electrode (red) surrounded by a shield (blue) on one plate and a high voltage electrode (red) surrounded by a shield (blue) on the other.

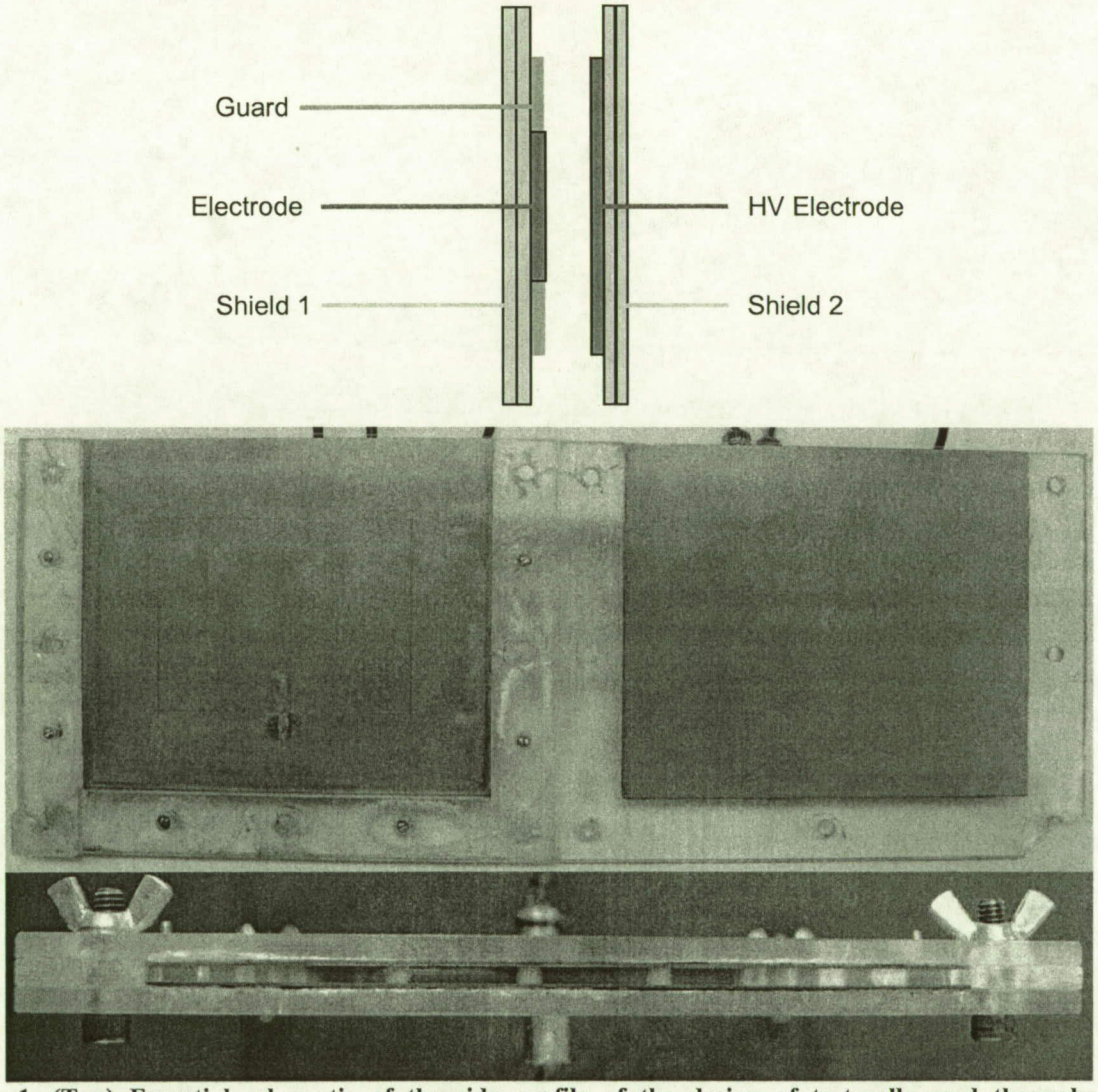

Figure 1. (Top) Essential schematic of the side profile of the design of test cells used throughout the experiments. (Bottom) Pictures of the Old Test Cell used to perform resistivity and charge decay measurements in dry environments. A top view of the final setup of the Old Test Cell is also shown.

The Old Test Cell is constructed using printed circuit boards with outside dimensions of 14 cm × 16.5 cm. The guarded electrode has dimensions of 10.2 cm × 7.6 cm with a guard gap between 0.1-0.2 mm. Surrounding the electrodes is a polycarbonate housing glued to the backside of the plates as shown in the bottom of Figure 1. The housing not only provides rigidity but also governs the spacing between the plates of 3.3 mm. For both plates, BNC wires are permanently attached to each side to serve as electrical connections for instrumentation (bottom of Figure 1).

Unlike the Old Test Cell, the New Test Cells were constructed using both square and round electrodes from printed circuit boards with a thickness of 1.53 mm (Figure 2). Square electrodes have dimensions of 4.43 cm × 4.43 cm and the round electrodes have diameters of 5 cm corresponding to electrode areas of 19.635 cm^2 as required by BS 5958. The guard for the square electrodes has dimensions of 7.0 cm × 7.0 cm while the guard for the round electrodes has a diameter of 7.5 cm. Each has a guard-electrode gap spacing of ~0.15 mm. The dimensions for the HV electrodes for both cells match the guard dimensions. The other side of the printed circuit board for both electrodes is completely coated with copper to act as a grounded shield. The spacing between the electrodes in both cases is held fixed at 5 mm by slots in a polycarbonate test fixture with inner dimensions of 9.5 cm × 9.5 cm that holds the circuit boards in place (Figure 2). Furthermore, the test specimen and the guard extend to at least twice as wide as the gap or sample thickness (> 1.0 cm), in accordance with ASTM D 150, in order to ignore edge effects completely. It is important to note that neither the edge of the HV electrode or the guard electrode extends to the polycarbonate fixture.

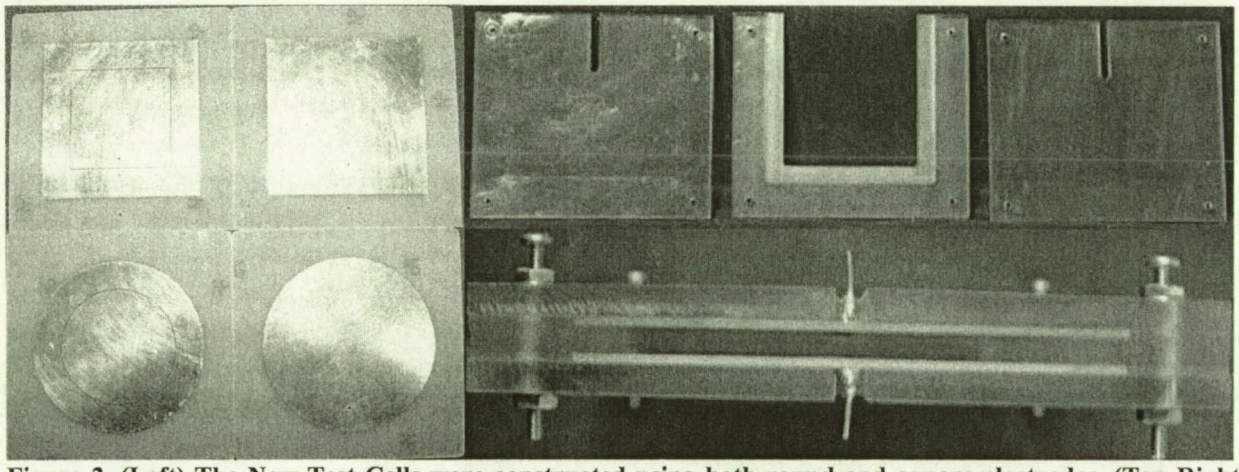

Figure 2. (Left) The New Test Cells were constructed using both round and square electrodes. (Top Right) The electrodes are sandwiched between a polycarbonate spacer and two backsides to form the cell. A top view of the cell is given in the bottom right.

An advantage of the New Test Cells is they contain pins that are soldered onto each metallic surface to allow for different cabling to attach to the test cell. This allows the electrical connection to the HV electrode plate to consist of 40 kV rated wire for both the HV Electrode and Shield 2, whereas the electrical connection for the electrode side consists of a modified triax cable with the electrode, guard and shield connected appropriately. These wires can then be connected to high vacuum feedthrus on the inside of the vacuum chamber and similar wires are connected to instrumentation on the outside of the chamber.

The ability to attach different cables to the New Test Cell is a major improvement over the Old Test Cell. One major limitation of the Old Test Cell is the low voltage rating of BNC wires limiting the applied voltage to 1300 volts. Resistivity measurements usually require higher voltages. Furthermore, the ability to use triax cable for current readings greatly reduces electrical noise compared to using two BNC cables tied together to function as a triax cable.

It should be noted that the Old Test Cell suffered from an electrical short between Shield 2 and the HV electrode. Although this is not a major concern for volume resistivity or dielectric measurements, chargeability tests are greatly affected and are not included for the Old Test Cell.

All tests were performed using Minnesota Lunar Simulant MLS-1 [21], which is believed to be a good lunar simulant because of its good mineralogical composition even without glass or agglutinates as a test material. The MLS-1 was sieved to particles of diameters between 50 and 75 μm and samples were dried out inside a vacuum for several days at 120°C before use.

In order to perfect the electrostatic measurement techniques before testing in vacuum, initial tests were performed in an environmental chamber (ETS Model 532 in Figure 3). Since moisture greatly affects electrostatic properties of granular materials, all tests using the Old Test Cell were performed inside the environmental chamber acclimating in pure GN_2 with a relative humidity below 0.1 %. Once the techniques were proven to work successfully under dry conditions using the Old Test Cell, experiments using the New Tests cells were moved inside a vacuum chamber to simulate lunar conditions (Figure 3). The vacuum chamber is fit with a Varian turbo pump (Turbo – V 300HT) capable of reaching pressures ~10^{-7} torr when empty.

Figure 3. (Left) The ETS environmental chamber used to house the Old Test Cell for electrostatic studies of MLS-1 under dry ambient conditions. (Right) The high vacuum chamber used to house the New Test Cells for testing under simulated lunar environmental conditions.

2.1 Faraday Cup or Chargeability Tests

The first results reported here are Faraday cup or chargeability tests performed under vacuum using the New Test Cells. These tests simulate the first of four tests performed by a flight instrument immediately during the filling operation. Each additional type of test requires different wiring connections to attach to different instrumentation. The dust inside the test cell

remains unchanged and all of the wiring changes can be done *outside* of the vacuum chamber as to not disturb the vacuum or the soil.

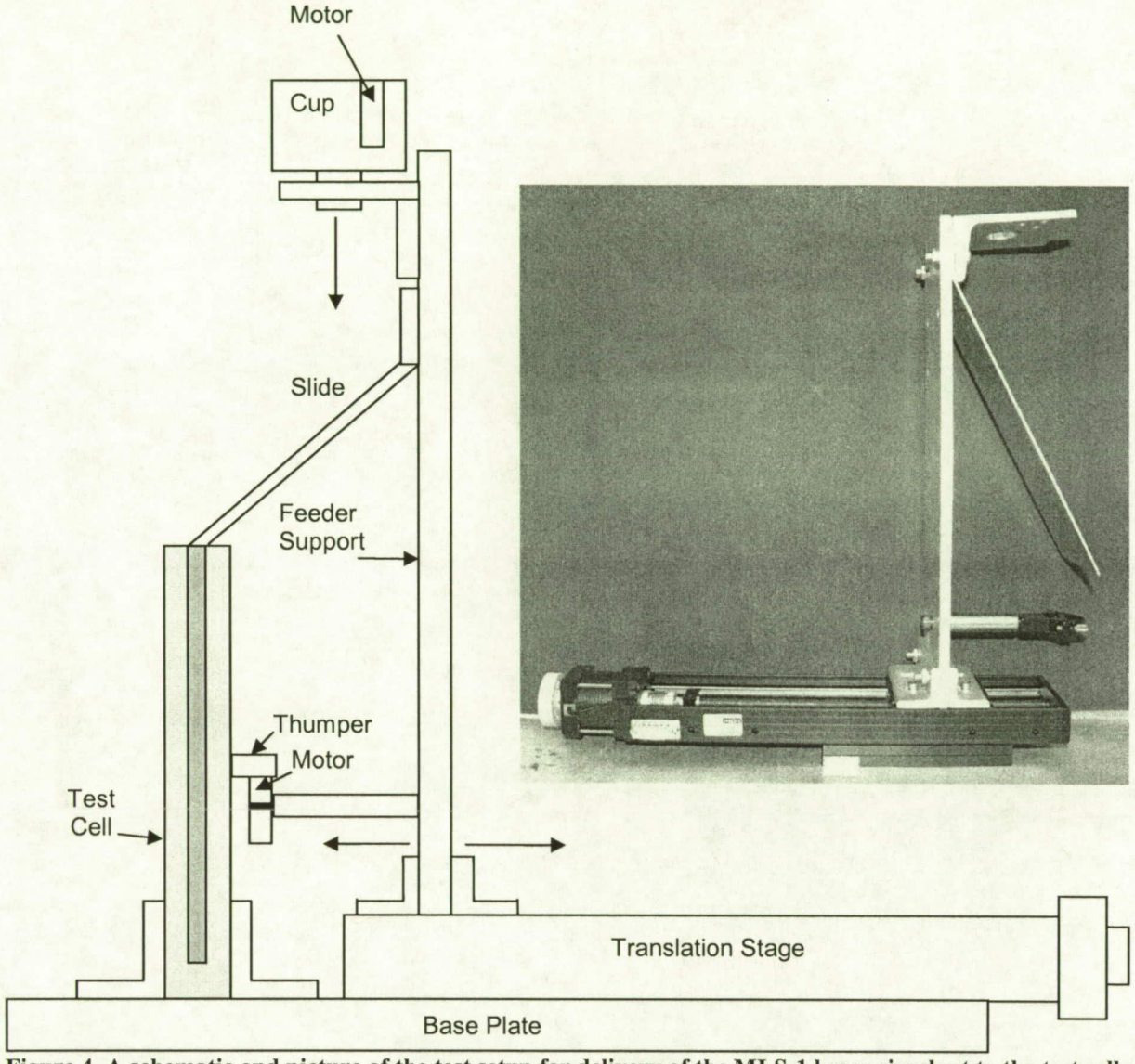

Figure 4. A schematic and picture of the test setup for delivery of the MLS-1 lunar simulant to the test cell.

In order to deliver the MLS-1 into the New Test Cell the following procedure was used. First, the baked out simulant was removed from the vacuum oven and placed inside a metal cup attached to a feeder support (see Figure 4). The vacuum chamber lid was shut and the chamber pumped down to 10^{-5} torr. While at vacuum, the feeder support attached to a translation stage was remotely controlled to move its slide directly over the opening of the test cell which is mounted (loosely) on the baseplate. Once in position, the motor attached to the metal cup was turned on which vibrates the cup and allows dust to flow onto the slide and into the cup. Once the cup was empty, a second motor with a thumper attachment was turned on to vibrate the test cell itself to allow complete dust settling in order to ensure consistent packing. After the test cell was filled, the feeder assembly was retracted along the translation stage.

For Faraday cup testing the two shields act to block out extraneous electric fields from the environment (which is why testing with the Old Test Cell does not work). The electric field lines of any charge inside of the test cell induce an equal and opposite charge on the HV and electrode surfaces that can be measured with a nanocoulomb meter. Typical nanocoulomb meters consist of an electrometer amplifier with a high quality capacitor connected in the negative feedback position as in Figure 5. The inverting input is at zero volts so that all charge that is induced is transferred directly to the integrating capacitor. Thus the voltage measured across the capacitor gives the charge of both the capacitor and the Faraday cup through $Q = CV$.

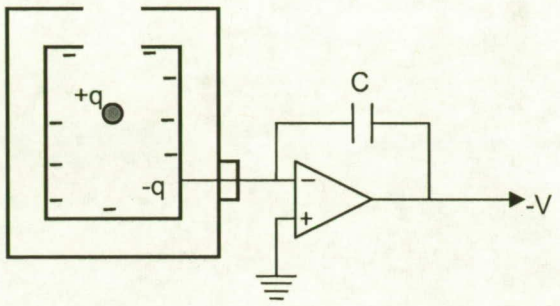

Figure 5. A schematic of a typical Faraday cup using a feedback electrometer scheme.

To transform our test cell into a Faraday cup, the guard, electrode and HV electrode were shorted together and connected to the center wire of a coax cable. The two shields were tied together and then connected to the outer coax line (ground). The coax cable was then plugged into a Model Number 284 Monroe Electronics (ME) Nanocoulomb meter. The notion of transforming a dielectric test cell into a Faraday cup is reported here for the first time.

Proof that the test cell operated as a Faraday cup was performed by simply immersing a charged object such as PTFE and recording the resulting charge with the ME Nanocoulomb meter. If the charge matched the value obtained by using the commercially available cup (ME Model 284/22B) then the test cell functions as a Faraday cup in this configuration. This was the case for our New Test Cell.

Two separate tests were performed using the dry MLS-1 simulant in order to verify the technique for measuring bulk charge-to-mass ratios. These experiments mimic how soils on the lunar surface may one day be handled, i.e. they could be lifted by a metal container and poured onto or into a sensitive device that may be damaged by high electrostatic fields. The ME Nanocoulomb meter was turned on and set to zero charge. The dust was allowed to flow and the resulting charge accumulation was measured. High charging could be expected since the dust is tribocharged by contact with a metallic surface (the slide) as it enters the test cell. The dust is allowed to flow until the holder cup is empty. The first measurement of charge taken after the dust has settled into the test cell with square electrodes was -189.6 μC for 61 grams of soil. A second test using the round electrodes gave -238.2 μC for the same amount of soil. This yields charge-to-mass ratios of -3.08 μC/kg and -3.88 μC/kg respectively. These are relatively high charging ratios for pouring actions but not unexpected in the low pressure high vacuum environment.

2.2 Dielectric Permittivity Measurements

The next series of tests performed on the MLS-1 while inside the New Test Cell under vacuum was dielectric permittivity measurements. Dielectric measurements were made consistent with ASTM Test Standard D 150 [20] across both electrodes in which the guard ring and the shields were grounded to reduce stray capacitances in the system. Measurements were taken using a QuadTech LCR Digibridge model 1730 which is capable of measuring capacitance, inductance, resistance, impedance as well as secondary parameters such as dissipation factor (tan δ), quality factor, equivalent series resistance, phase angle and reactance at ten different frequencies: 50 Hz, 60 Hz, 100 Hz, 120 Hz, 1 kHz, 10 kHz, 20 kHz, 40 kHz, 50 kHz and 100 kHz. Here we are focusing on measurements of the capacitance and the dissipation factor only.

LCR meters are based on four terminal Kelvin connections in which a signal generator outputs a signal at a given frequency and a certain voltage between two terminals IH and IL while a current sensing resistor R_S is used to measure the current flowing between them. The basic LCR schematic is shown in Figure 6.

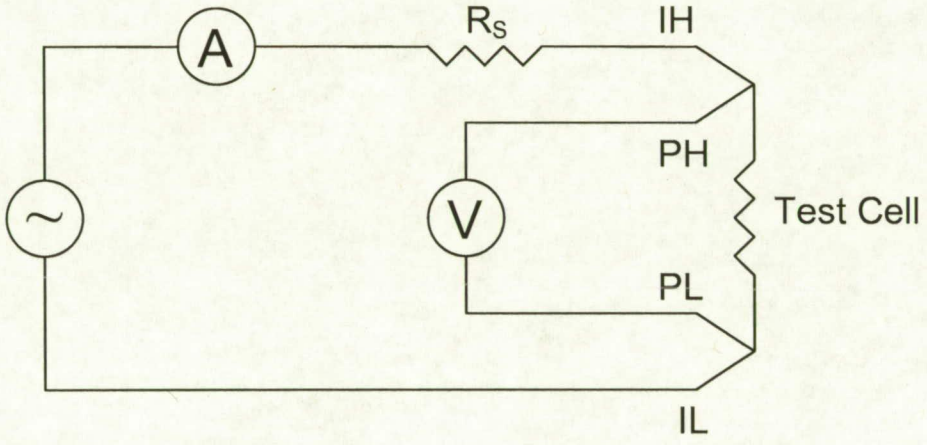

Figure 6. A simplified schematic of an LCR Meter.

The voltage is measured between PH and PL which has a high input impedance so that little or no current flows between these terminals. This configuration allows the instrument to measure both current and voltage across the test cell accurately. In order to get the permittivity of the dust we first had to take measurements of the empty cell. Table 2 shows the values for the dielectric constant for MLS-1 simulant using both electrode geometries.

Measurements at frequencies below 1 kHz were fluctuating and maybe somewhat unreliable while values at and above 1 kHz were stable and did not fluctuate in time. The dielectric constant did not change with frequency, suggesting the absence of moisture. In addition, the measurements of the dissipation factor $\tan\delta$ were very small as suggested by the literature. The New Test Cells show that the soil is a very good electrical insulator with a dielectric constant of about 4.

Table 2. Dielectric Permittivity measurements of MLS-1 using New Test Cells

	Empty Cell Square Electrodes		MLS -1 Square Electrodes		
Frequency (Hz)	Capacitance (pF)	Tan δ	Capacitance (pF)	Tan δ	Dielectric Constant
50	3.9	0	17.8	0.045	4.56
60	3.9	0	17.8	0.045	4.56
100	3.8	0	17.6	0.045	4.63
120	3.9	0	17.6	0.045	4.51
1000	3.92	0	17.02	0.0213	4.34
10,000	3.93	0	16.66	0.0141	4.24
20,000	3.97	0	16.73	0.0145	4.21
40,000	3.94	0	16.51	0.013	4.19
50,000	3.96	0	16.55	0.0127	4.18
100,000	4.074	0.0041	16.94	0.016	4.16
AVERAGE	**3.9294**	**0.00041**	**17.121**	**0.02716**	**4.36**
	Empty Cell Round Electrodes		**MLS -1 Round Electrodes**		
Frequency (Hz)	Capacitance (pF)	Tan δ	Capacitance (pF)	Tan δ	Dielectric Constant
50	4	0.2	16.6	0.0256	4.15
60	5.7	0.3	17	0.42	2.98
100	3.6	0.002	16.7	0.0339	4.64
120	3.6	0.01	16.6	0.0368	4.61
1000	3.65	0.0001	16.05	0.0205	4.40
10,000	3.66	0.0001	15.72	0.0133	4.30
20,000	3.69	0.0001	15.76	0.0135	4.27
40,000	3.67	0.0001	15.58	0.012	4.25
50,000	3.68	0.0001	15.6	0.012	4.24
100,000	3.78	0.0035	15.9	0.014	4.21
AVERAGE	**3.903**	**0.0516**	**16.151**	**0.06016**	**4.20**

The values of the dielectric constant taken with the MLS-1 under vacuum using the New Test Cells were compared with those taken with the Old Test Cell under low humidity. MLS-1 was not loaded in the Old Test Cells using a dust feeding system. Instead the dust from the vacuum oven could be loaded manually using a funnel. The results of the dielectric constant using the Old Test Cell are listed in Table 3.

Although the results for the dielectric constant in the Old Test Cell are not identical to those using the New Test Cells, the values are still consistent with the literature ~3-5. Measurements of the dissipation factor were not taken with the Old Test Cells.

Table 3. Dielectric Permittivity measurements of MLS-1 using Old Test Cells

	Empty Old Test Cell	MLS-1 Filled Old Test Cell	
Frequency (Hz)	Capacitance (pF)	Capacitance (pF)	Dielectric Constant
50	21.6	56.4	2.61
60	21.6	60.9	2.80
100	21.6	58.3	2.69
120	21.6	58.3	2.69
1000	21.6	57.26	2.65
10,000	21.6	56.81	2.60
20,000	21.6	57.89	2.65
40,000	21.6	56.73	2.60
50,000	21.6	57.08	2.65
100,000	21.6	60.51	2.80
AVERAGE	**21.6**	**58.018**	**2.674**

2.3 Direct Volume Resistivity Measurements

For some materials with extremely high resistivities $>10^{10}\,\Omega$m, the application of voltage across them results in a current that decreases with time. This decrease in current which appears to be an increase in resistivity, can last for several hours in a process known as polarization. This process may have several origins including limited dipole response, exhaustion of charge carriers, electrode effects, charge trapping, etc...[22] The question then arises as to when is the best time to sample the current. Generally, resistivity measurements should be taken after several minutes, once the current is stabilized if possible.

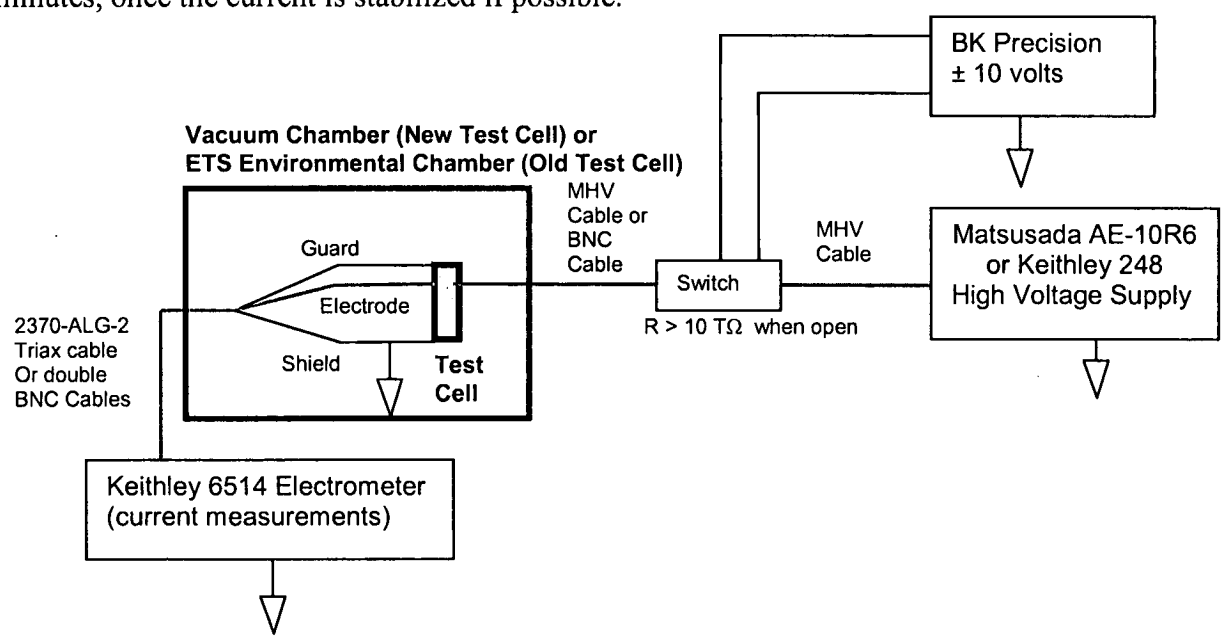

Figure 7. Schematic of the experimental setup used to measure the resistivity of MLS-1 for both the New Test Cell and the Old Test Cell.

Test cell configurations for resistivity experiments were as follows (see Figure 7). Measurements using the Old Test Cell were performed inside the ETS chamber while tests using the New Test Cells were performed inside the vacuum chamber of Figure 3. The Matsusada Voltage Power Supply model AE-10R6 supplied high electrostatic potentials to the high voltage electrode of the New Test Cell, while a Keithley 248 provided high voltage for the Old Test Cell. For the New Test Cell, electrical connections are made using a MHV cable through a 30 kV rated high vacuum feedthru. There is a high voltage ceramic switch (rated at 7 kV) in series with the HV wire to allow an electrical open or closed circuit between the Matsusada and the HV electrode of the test cell. The switch is operated using a BK Precision power supply. For the New Test Cells, shield 2 on the high voltage side was left floating to prevent breakdown across or through the printed circuit board. To measure the current through the soil, the guard, electrode and shield 1 are comprised of a triax cable connected to the triax input of a Keithley 6514 Electrometer. Great care was taken to ensure that residual electric fields were not inducing extraneous currents. Outside fields were shielded using copper mesh surrounding the Keithley 6514 to minimize electrical noise to a level of a few picoamps. The voltage on the Matsusada and the current from the Keithley 6514 were all monitored by National Instruments Ni-Daq card and read using LabView.

In the case of the Old Test Cell, shield 2 was electrically shorted to the HV wire which does not pose a problem as mentioned earlier. For current measurements, the Old Test Cell contained two BNC outputs on the electrode side (one for the electrode and one for the guard) the guard had to be shorted to ground and the current was monitored through the electrode. The BNC connection to the Keithley 6514 Electrometer forced the guard setting on the instrument to be turned off.

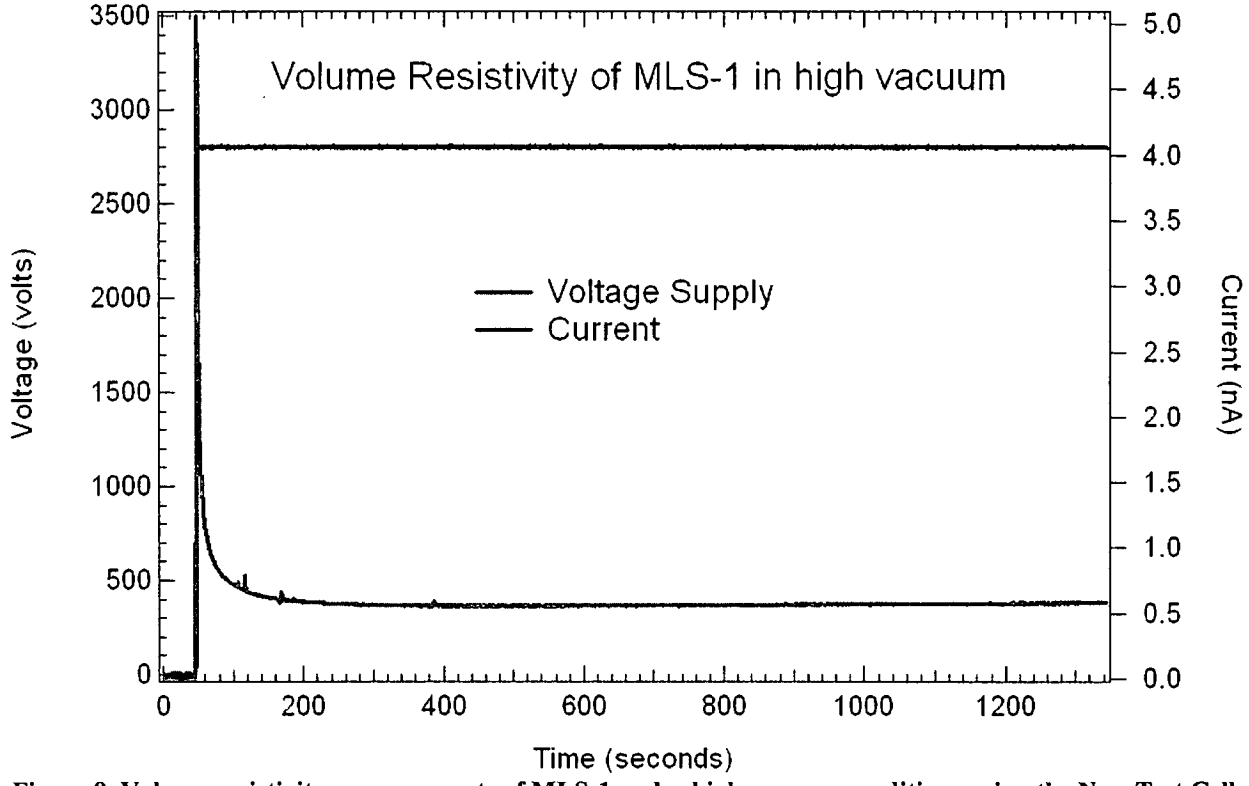

Figure 8. Volume resistivity measurements of MLS-1 under high vacuum conditions using the New Test Cell.

Volume resistivity measurements are performed by simply applying a known voltage, recording a stable current, and multiplying the value by the appropriate cell constant. Direct measurements of volume resistivity were not possible using the Old Test Cells with BNC wires to supply HV since the lower voltage (limited to ~1300 volts) did not provide a stable current. Thus these wires were replaced with HV wire rated at 30 kV in the design of the New Test Cell to allow for higher supplied voltage. However, it is possible to extract values of resistivity from charge decay measurements discussed in the next section.

Volume resistivity measurements were successful using the New Test Cells with higher than 1500 volts applied. An example test is given in Figure 8. Voltages above 3700 were not used due to electrical breakdown across the gap. Experiments were performed to record the background noise of 10^{-14} A giving a lower limit of current that can be detected. The area to distance ratio, or cell constant, of the New Test Cells is (19.635 cm^2)/(0.5 cm) = 39.25 cm = 0.3925 m. All experiments were performed at 10^{-5} torr. The measured volume resistivities using the New Test Cell are given in Table 4. The red highlighted test was the measurement shown in Figure 8.

Table 4. Volume Resistivity Measurements of MLS-1 using the New Test Cell

Voltage (v)	Current (A)	Resistance (Ω)	Resistivity (Ωm)
1690	2.10E-10	8.04762E+12	3.15867E+12
2170	4.10E-10	5.29268E+12	2.07737E+12
2810	5.70E-10	4.40351E+12	1.72837E+12
2940	1.10E-09	2.67273E+12	1.04904E+12
3330	1.70E-09	1.95882E+12	7.68834E+11
Average		**4.47507E+12**	**1.75646E+12**

All volume resistivity values fall within the appropriate range for highly insulating silicate materials and are consistent with the literature for lunar fines.

Previous authors such as Olhoeft [1] designed a test cell that housed only 2.5 grams of lunar soil built to the same ASTM standards used here, that was successful in measuring stable currents below 1300 volts. He and other authors were able to make successful measurements at lower voltages using commercially available instrumentation such as the Hewlett-Packard Model 4329A [1, 2]. This device is limited to 1000 test volt output, which was clearly not sufficient for resistance measurements with either of our test cells. It is important to note that it is our experience that measurements performed on such small samples ~2 grams do not necessarily correlate with those of larger samples when keeping the dimensional ratios equivalent. Thus the area-to-distance ratio held fixed does not guarantee that the volume resistivity will follow for smaller sample sizes due to the variations discussed above. We believe that one should comply with the ASTM standards (which does not specify cell dimensions but the guard/electrode design) and also the British Standard 5958 [19] which specifies the spacing, size and amount of material. For it is in this case only that researchers elsewhere can compare volume resistivity measurements of granular materials successfully.

2.4 Charge Decay Measurements

Charge decay was the final measurements taken with the MLS-1 simulant. Previous studies used *corona* charging to provide charge to the surface of granular materials [8, 9] but here we use a new method called *induction* charging to supply the necessary charge to the soil. This method is loosely based on an old standard Federal Test Method 101C Method 4046 [23]. Induction charge occurs when high voltages are applied to metallic surfaces, electrons may become transferred to adjacent insulating surfaces.

Charge decay was performed by applying a voltage to the HV electrode, disconnecting the HV power supply from the circuit, and monitoring the resulting potential decay of the HV electrode. Any charge dissipation of the HV electrode must have occurred as a result of charge transferring through the test material inside the test cell provided it is the material with the least intrinsic electrical resistance. Charge must not be allowed to "leak" away through other surfaces to ground which is extremely difficult experimentally.

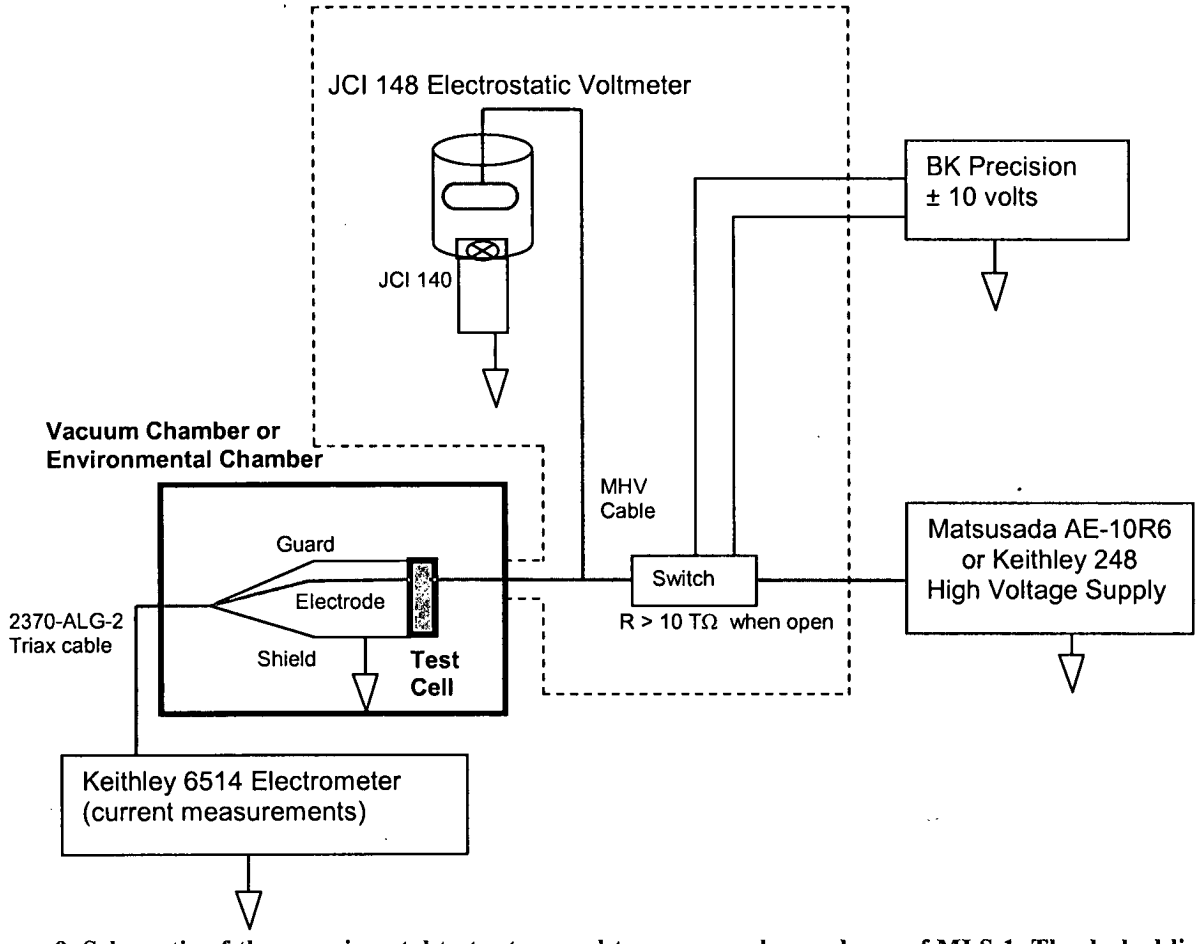

Figure 9. Schematic of the experimental test setup used to measure charge decay of MLS-1. The dashed line represents equipment housed in a very low humidity environment (RH < 1.0%).

The basic method used to measure charge decay by induction is shown in Figure 9. The charge decay tests are performed immediately following resistivity measurements using the identical

setup mentioned previously. The only addition is a model JCI 148 Electrostatic Voltmeter in parallel with the HV electrode of the test cell. The JCI 148 consists of a large shielded brass electrode held to the same potential as the HV electrode whose potential is measured accurately using a JCI 140 Fieldmeter. It has a very large internal capacitance of 7 pF which isolates it from the system. The design of the JCI 148 allows accurate measurements of high electrostatic voltages shielded from the environment with virtual no charge leakage. One advantage of measuring charge decay and resistivity with the Old Test Cell is that much of the equipment is housed inside the ETS environmental chamber along with the test cell. The voltage on the Keithley 248, the JCI 148 and the current from the Keithley 6514 were all monitored by National Instruments Ni-Daq card and read using LabView.

An example of how both resistance and charge decay measurements can be made during the same set of experimental runs is shown in Figure 10 below for dry MLS-1 using the Old Test Cell. All that is required is to turn off the HV switch, disconnect the HV power supply and monitor the voltage on the HV electrode using the JCI 148. Charge decays through the soil and is continuously monitored using the Keithley 6514. A full experiment begins by closing the switch and turning the Matsusada to a preset voltage corresponding to time #1 of Figure 10. Resistance measurements can be made by monitoring the current during the applied voltage phase at time #2. However, for charge decay measurements the switch is opened at time #3 and the wires connecting to the switch from the BK Precision as well as the MHV cable connecting the Keithley 248 are disconnected and removed to ensure that the only electrical ground path is through the MLS-1 soil.

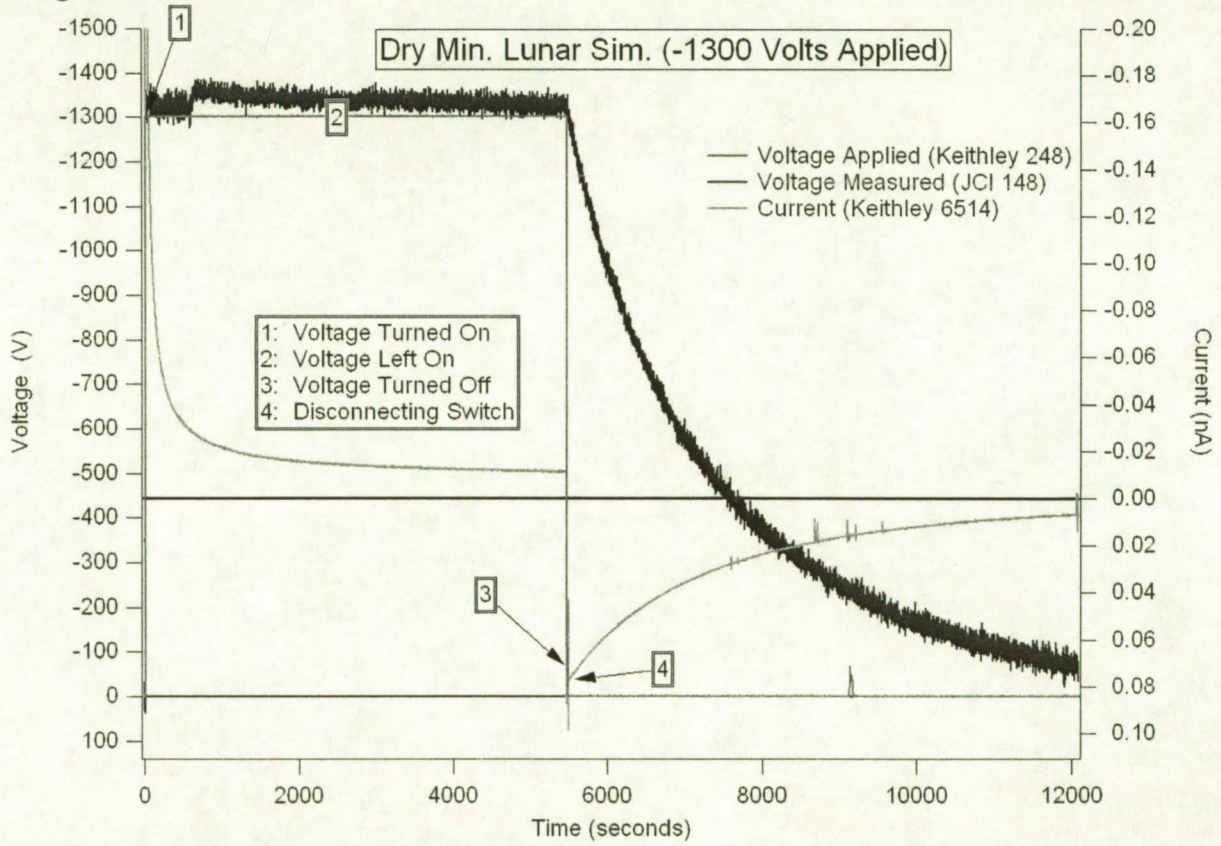

Figure 10. A sample data set showing the voltage applied (red), the voltage monitored using the JCI 148 (blue) and the current measured with the Keithley 6514 (green) for the Old Test Cell.

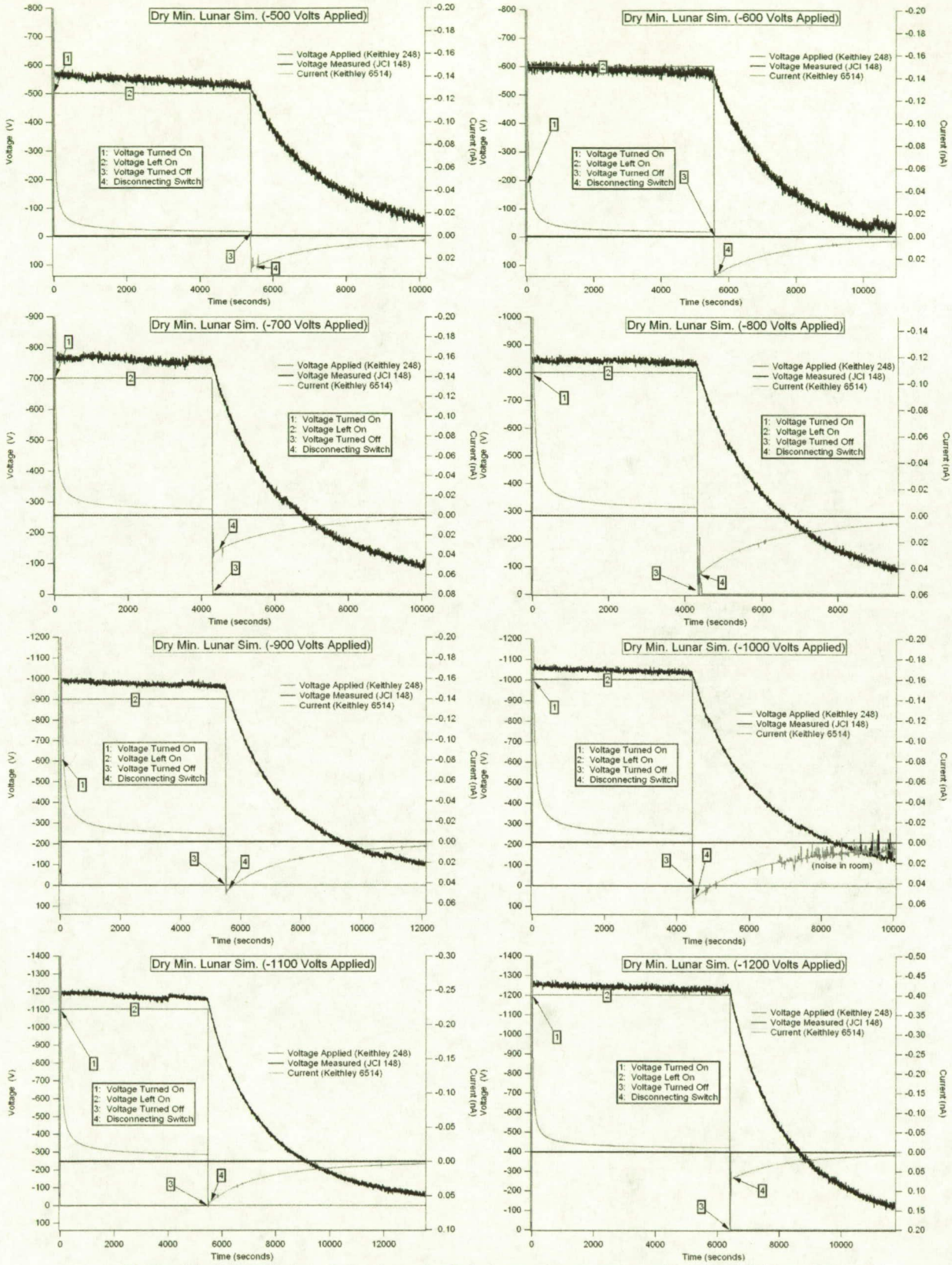

Figure 11. Several data sets of successful charge decay runs using the Old Test Cell.

For resistivity measurements with a low voltage applied, 100 minutes is still not enough time for the current to stabilize as seen in Figure 10 (at #3). However, valuable information is still available in the form of the electrostatic charge decay curve after time #4. The experiment is allowed to run for long periods of time after the voltage has been turned off to ensure that the voltage has fallen below 37% (1/e) of its initial value. Several more data sets with a negative applied voltage are given in Figure 11 using the Old Test Cell.

Similar tests were performed under high vacuum conditions using the New Test Cells. An extremely important feature is that the JCI 148, JCI 140, high voltage switch and the MHV cables connected to the HV electrical feedthrus must be housed in a low humidity environment, one continually purged with dry nitrogen, to ensure that charge leakage as a result of moisture accumulation does not occur. For the vacuum system, as in the case for the New Test Cells, two smaller acclimation chambers had to be built separately; one to house the JCI 148, JCI 140 and the HV switch and another separate chamber to house the +30 kV rated electrical feedthru for the HV cable. Even the smallest amount of moisture in air can settle on surfaces and serve as an unwanted ground path if not properly contained. Several examples of resistance and charge decay plots are shown in Figure 12. Note that in these cases the current did stabilize to provide the resistivity data in Table 4.

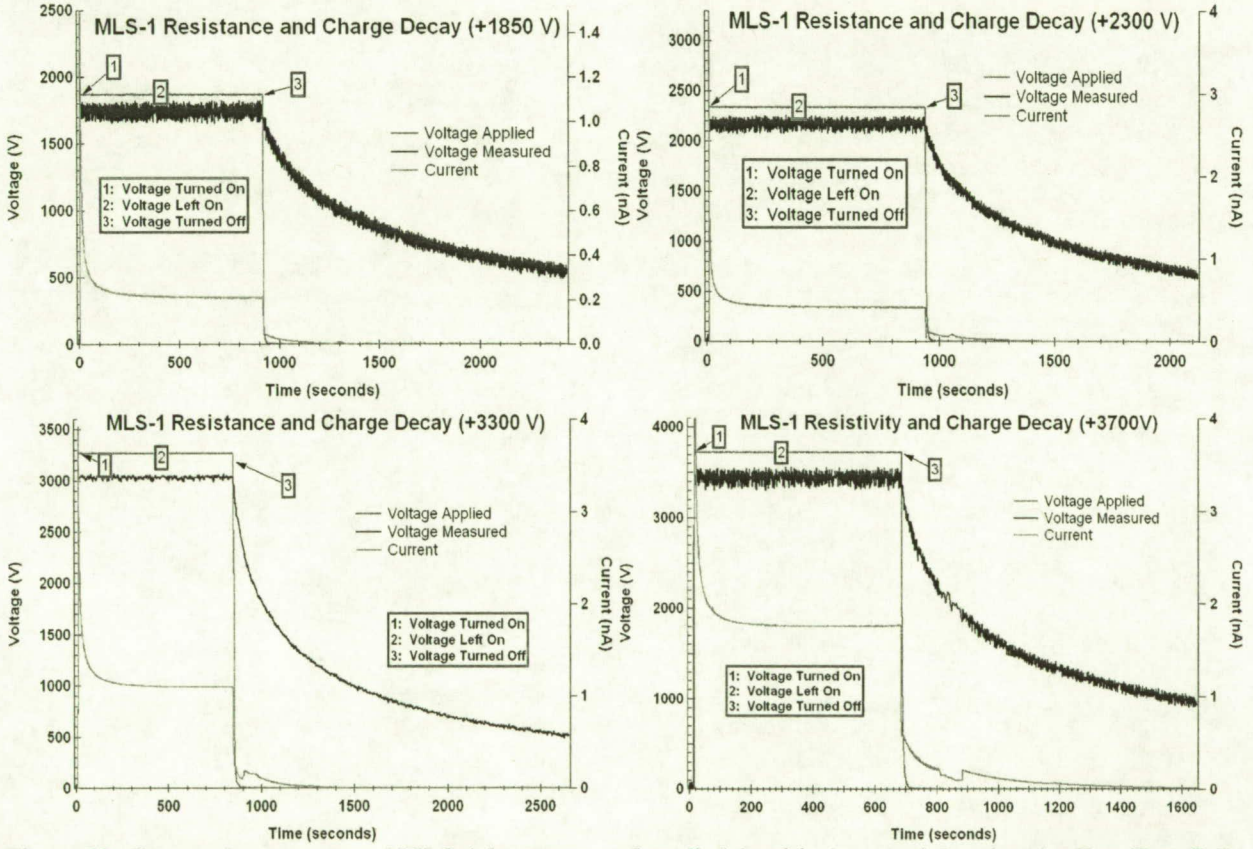

Figure 12. Charge decay curves of MLS-1 for a range of applied (positive) potentials using the New Test Cell under high vacuum conditions.

The form of the charge decay is not a simple Ohmic charge decay behavior as seen for purely capacitive and resistive systems. IGOR was used to fit the data to (1) exponential decay, (2) hyperbolic decay and (3) Seaver's generalized equation mentioned in the introduction. The fits

were performed by a regression analysis in which constant parameters were allowed to fluctuate. If the initial guesses of the choice parameters was accurate, the fit would converge successfully. Only a few passes (<10) were normally required for an accurate fit. An example of a Seaver fit to the experimental data is given in Figure 13.

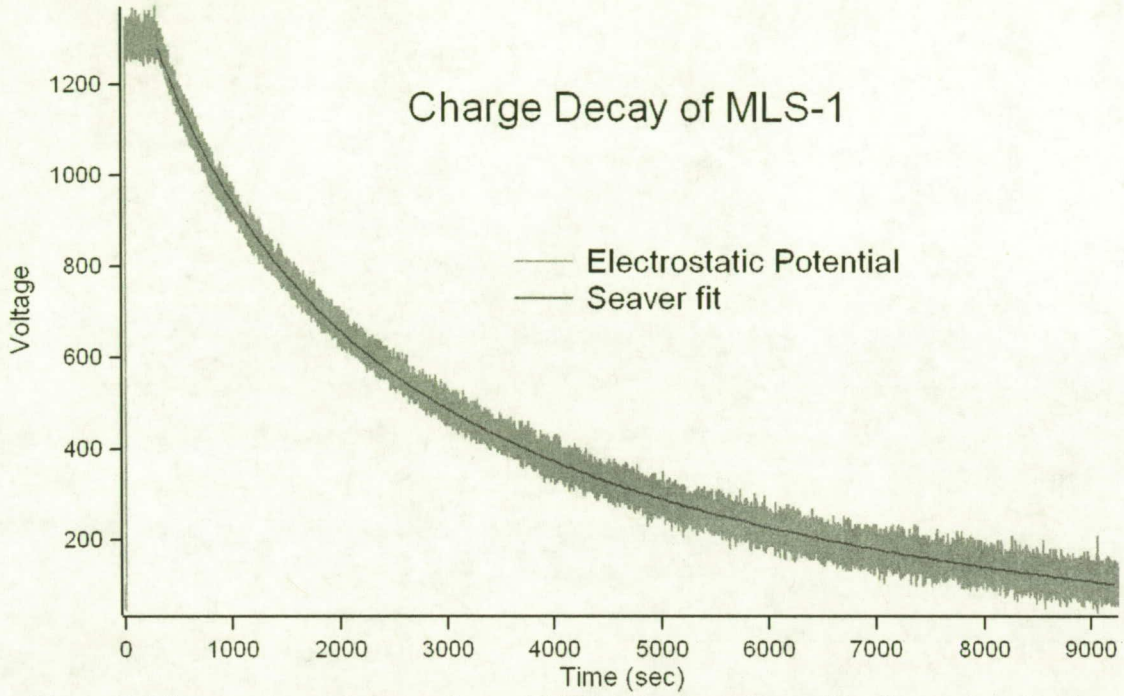

Figure 13. The experimental charge decay of MLS-1 simulant along with a Seaver function data fit.

Other fits to the data including exponential decays and hyperbolic decays did not match as well but were included in the final analysis. To reiterate the equations used for the fits:

Seaver Analysis:

$$\rho_{Seavor}(t) = \frac{\rho_{p0}}{\left(1+\frac{\tau_m}{\tau_p}\right)\exp\left(t/\tau_m\right) - \frac{\tau_m}{\tau_p}}$$ with $\tau_m = \frac{\varepsilon}{\sigma_m} = R_v \varepsilon$ and $\tau_p = \frac{\varepsilon}{b_p \rho_{p0}}$ providing information on the conductivity, resistivity and the mobility.

Exponential Decay:

$$\rho_{Exp}(t) = \rho_{p0}\exp(-t/\tau_m)$$ with $\tau_m = \frac{\varepsilon}{\sigma_m} = R_v \varepsilon$ providing information on the conductivity and resistivity.

Hyperbolic Decay:

$$\rho_{Hyp}(t) = \frac{\rho_{p0}}{\left(1+\frac{t}{\tau_p}\right)}$$ with $\tau_p = \frac{\varepsilon}{b_p \rho_{p0}}$ providing information on the charge mobility.

Table 4. Seaver, exponential and hyperbolic fits to the charge decay curves.

Voltage (V)	Seaver Analysis			Exponential Decay		Hyperbolic Decay	
	τ_m (sec)	τ_p (sec)	ρ_0 (C/m^3)	τ (sec)	ρ_0 (C/m^3)	τ (sec)	ρ_0 (C/m^3)
500	1.915E+04	2.982E+03	1.063E-03	3.159E+03	1.063E-03	2.737E+03	1.063E-03
600	3.563E+03	2.367E+03	1.276E-03	2.998E+03	1.276E-03	2.878E+03	1.276E-03
750	3.429E+04	2.564E+03	1.594E-03	2.926E+03	1.594E-03	2.431E+03	1.594E-03
850	7.546E+03	2.844E+03	1.807E-03	2.849E+03	1.807E-03	2.132E+03	1.807E-03
1000	1.246E+04	2.164E+03	2.126E-03	2.691E+03	2.126E-03	1.919E+03	2.126E-03
1100	3.792E+03	2.758E+03	2.339E-03	3.428E+03	2.339E-03	2.000E+03	2.339E-03
1200	1.378E+04	2.293E+03	2.551E-03	2.589E+03	2.551E-03	2.064E+03	2.551E-03
1300	6.985E+03	2.179E+03	2.764E-03	2.793E+03	2.764E-03	1.590E+03	2.764E-03
1850	6.215E+02	1.672E+01	3.049E-03	5.034E+02	3.049E-03	4.367E+02	3.049E-03
2300	4.008E+02	1.875E+02	3.791E-03	3.774E+02	3.791E-03	5.854E+02	3.791E-03
3300	4.823E+02	4.730E+01	5.439E-03	3.743E+02	5.439E-03	5.836E+02	5.439E-03
3700	2.620E+02	1.020E+02	6.098E-03	2.532E+02	6.098E-03	4.498E+02	6.098E-03
	Resistivity (Ωm)	Conductivity (S/m)		Resistivity (Ωm)	Conductivity (S/m)		
500	8.303E+14	1.204E-15		1.370E+14	7.300E-15		
600	1.545E+14	6.472E-15		1.300E+14	7.692E-15		
750	1.487E+15	6.725E-16		1.269E+14	7.881E-15		
850	3.272E+14	3.056E-15		1.235E+14	8.094E-15		
1000	5.403E+14	1.851E-15		1.167E+14	8.570E-15		
1100	1.644E+14	6.081E-15		1.486E+14	6.727E-15		
1200	5.977E+14	1.673E-15		1.123E+14	8.907E-15		
1300	3.029E+14	3.301E-15		1.211E+14	8.257E-15		
1850	1.697E+13	5.893E-14		1.375E+13	7.275E-14		
2300	1.094E+13	9.137E-14		1.031E+13	9.704E-14		
3300	1.317E+13	7.593E-14		1.022E+13	9.784E-14		
3700	7.154E+12	1.398E-13		6.913E+12	1.447E-13		
	Mobility (m^2/Vs) $\mu = \varepsilon/(\rho_0 \cdot \tau_p)$					Mobility (m^2/Vs) $\mu = \varepsilon/(\rho_0 \cdot \tau)$	
500	7.275E-12					7.926E-12	
600	7.638E-12					6.282E-12	
750	5.641E-12					5.949E-12	
850	4.487E-12					5.986E-12	
1000	5.013E-12					5.653E-12	
1100	3.575E-12					4.931E-12	
1200	3.942E-12					4.380E-12	
1300	3.829E-12					5.248E-12	
1850	7.184E-10					2.751E-11	
2300	5.153E-11					1.651E-11	
3300	1.424E-10					1.154E-11	
3700	5.888E-11					1.335E-11	

The final results for all of the charge decay runs are provided in Table 4. The red values indicate those from the New Test Cell while the black values correspond to Old Test Cell data. The initial charge density values ρ_0 are derived from the initial charge values divided by the volume of the test cell. Hence

$$\rho_0 = \frac{Q}{Vol} = \frac{VC}{Vol}$$

where the initial charge values are given by $Q = VC$ for a parallel plate capacitor where V is te applied voltage, C is the capacitance of the test cell (given in Tables 2 and 3), and Vol is the volume of the respective test cell. The conditions for a good insulator as met using $\tau_p < \tau_m$ by at least an order of magnitude according to Table 4 for the Old Test Cell. The coefficient fits for the resistivities given by Seaver and exponential decays match well in all cases. Additionally, the coefficient fits for the mobilities given by the Seaver and hyperbolic decays match well. The values of the mobility in both the Seaver analysis and the hyperbolic limit are well within the range of expected charge carriers in insulating materials. The values of resistivity taken with the Old Test Cells compared to the New Test Cells are slightly higher. Although we ignored resistivity values taken with the Old Test Cells since the current did not stabilize at the lower voltages, the resistivity values extracted from charge decay fits match the values of the resistivity calculated from current at the point of the initial charge decay measured at the time when the voltage decay was initiated. For example, the value at which the current is read at ~500 seconds in Figure 10 which corresponds to #3 is about ~10 pA. This current correlates to a volume resistivity of $\sim 5 \times 10^{13}$ Ωm. In either case, the fits to the charge decays give similar magnitudes both of which are well within reported values of resistivity for lunar soils.

3.0 References

1. Olhoeft, G.R., A.L. Frisillo, and D.W. Strangway, *Electrical Properties of Lunar Soil Sample 15301,38.* Journal of Geophysical Research, 1974. **79**(11): p. 1599-1604.
2. Alvarez, R. *Lunar and terrestrial sample photoconductivity.* in *Proceedings of the 6th Lunar Science Conference.* 1975. Houston, TX: NASA Astrophysics Data System.
3. Olhoeft, G.R., et al., *Temperature dependence of electrical conductivity and lunar temperatures.* The Moon, 1974. **9**: p. 79-87.
4. Olhoeft, G.R. and D.W. Strangway, *Dielectric Properties of the First 100 Meters of the Moon.* Earth and Planetary Science Letters, 1975. **24**: p. 394-404.
5. Seaver, A.E. *An Equation for Charge Decay Valid in Both Conductors and Insulators.* in *Proceedings of the ESA-IEJ Joint Meeting of Electrostatics.* 2002. University of Arkansas at Little Rock.
6. Bustin, W.M., I. Koszman, and I.T. Tobye, *A new theory of static relaxation.* Hydrocarbon Processing, 1964. **43**: p. 209-216.
7. J.M., C., *Fundamentals of Applied Electrostatics.* 1986, New York: John Wiley & Sons.
8. Buhler, C.R., et al. *Charge Decay Characteristics of the JSC Mars-1 Martian Regolith Simulant.* in *Proceedings of the 39th Space Congress.* 2002. Cape Canaveral, FL.
9. Buhler, C.R., et al. *Non-Ohmic Discharge Characteristics of JSC Mars-1 Martian Regolith Simulant.* in *Lunar and Planetary Science Conference XXXIII.* 2002. Houston, TX.
10. Chubb, *New approaches for electrostatic testing of materials.* Journal of Electrostatics, 2002. **54**: p. 233-244.
11. Freeman, J.W. and M. Ibrahim, *Lunar electric fields, surface potential and associated plasma sheaths.* The Moon, 1975. **8**: p. 103-114.
12. Berg, O.E., F.F. Richardson, and H. Burton, *Lunar ejecta and meteorites experiment.* Apollo 17 Preliminary Science Report (NASA SP-330), 1973: p. 16-1.
13. Colwell, J.E., et al., *The Lunar Surface: Dust Dynamics and Regolith Mechanics.* Reviews of Geophysics (submitted), 2006.
14. Nitter, T., O. Havnes, and F. Melandso, *Levitation and dynamics of charged dust in the photoelectron sheath above surfaces in space.* Journal of Geophysical Research, 1998. **103**: p. 6605-6620.
15. Robertson, S., et al., *Dust grain charging and levitation in a weakly collisional sheath.* Physics of Plasmas, 2003. **10**: p. 3874-3880.
16. Arnas, C., M. Mikikian, and F. Doveil, *Micro-Sphere levitation in a sheath of a low pressure continuous discharge.* Physica Scripta, 2001. **T89**: p. 163-167.
17. Sickafoose, A.A., et al., *Experimental levitation of dust grains in a plasma sheath.* Journal of Geophysical Research, 2002. **107**: p. doi:10.10299/2002JA009347.
18. Grard, R.J.L. and J.K.E. Tunaley, *Photoelectron sheath near a planetary probe in interplanetary space.* Journal of Geophysical Research, 1971. **76**: p. 2498-2505.
19. BSi, *Code of practice for Control of undesirable static electricity.* BS 5958, 1991. **Part 1**.
20. ASTM, *Standard Test Method for AC Loss Characteristics and Permittivity (Dielectric Constant) of Solid Electrical Insulation.* ASTM D 150 - 98 2004.
21. Weiblen, P.W. and K. Gordon, *Second Conference on Lunar Bases and Space Activities of the 21st Century.* Lunar and Planetary Science Contribution 652, 1988.

22. Taylor, D.M. and P.E. Secker, *Industrial Electrostatics*. Research Studies Press LTD. 1994, Taunton, Somerset, England: John Wiley & Sons Inc.
23. *United States Federal Test Standard 101C Test Method 4046.* EIA Interim Standard 1S-5-A.